SOFT ROBOTICS
Volume 11, Number 6, 2024
© Mary Ann Liebert, Inc.
DOI: 10.1089/soro.2023.0177

SoRo
Soft Robotics

Open camera or QR reader and scan code to access this article and other resources online.

ORIGINAL ARTICLE

A Reconfigurable Soft Linkage Robot via Internal "Virtual" Joints

Mingsong Jiang,* Jiansong Wang,† and Nicholas Gravish

Downloaded by UNIVERSITY OF CALIFORNIA SAN DIEGO from www.liebertpub.com at 01/14/25. For personal use only.

Abstract

Traditional robots derive their capabilities of movement through rigid structural ''links'' and discrete actuated ''joints.'' Alternatively, soft robots are composed of flexible materials that permit movement across a continuous range of their body and appendages and thus are not restricted in where they can bend. While trade-offs between material choices may restrain robot functionalities within a narrow spectrum, we argue that bridging the functional gaps between soft and hard robots can be achieved from a hybrid design approach that utilizes both the reconfigurability and the controllability of traditional soft and hard robot paradigms. In this study, we present a hybrid robot with soft inflated ''linkages,'' and rigid internal joints that can be spatially reconfigured. Our method is based on the geometric pinching of an inflatable beam to form mechanical pinch-joints connecting the inflated robot linkages. Such joints are activated and controlled via internal motorized modules that can be relocated for on-demand joint–linkage configurations. We demonstrate two applications that utilize joint reconfigurations: a deployable robot manipulator and a terrestrial crawling robot with tunable gaits.

Keywords: reconfigurable soft robots, inflatable robots, pinch-joint mechanism, untethered actuation

Introduction

Traditional hard robots are constructed of rigid links and distinct joints, facilitating direct control and simplifying system actuation.[1,2] They are made of stiff materials and actuated by powerful mechanisms, allowing them to support large forces while adhering to theoretical kinematics.[3,4] However, this leads to high inertia and potential environmental impacts.[5,6] In contrast, the field of soft robotics has emerged where elastomeric materials[7–9] and flexible yet field-responsive sensors[10–12] and actuators[13,14] have been largely explored to build a myriad of soft machines.[7,15–19] These robots leverage highly compliant and adaptable materials to demonstrate simplified yet programmable biomorphic kinematics,[20–22] surface sensing,[23,24] tunable stiffness,[19,25] and varied morphologies,[17,26] among other features.[27,28] Design approaches in soft robotics excel in scenarios requiring safe human–robot interactions,[29,30] lightweight and deployable robots,[31,32] and adaptability to varied environments.[33,34]

While traditional soft robots offer flexibility, they encounter challenges such as unregulated degrees of freedom,[35,36] limited structural strength and force production,[13,37] and sustainable energy source issues,[38,39] all potentially affecting their performance.[40,41] Much research focuses on enhancing

Department of Mechanical and Aerospace Engineering, University of California San Diego, La Jolla, California, USA.
*Current address: Department of Mechanical Engineering and Materials Science, Yale University, New Haven, Connecticut, USA.
†Current address: Department of Mechanical Engineering, Carnegie Mellon University, Pittsburgh, Pennsylvania, USA.

soft components such as reinforced actuators[42–44] and high-energy-density materials.[45,46] Yet, the potential of integrating heterogeneous robot components can be exploited to augment soft robot applications. Examples include a large-scale untethered robot with a reconfigurable frame,[47] incorporation of both rigid and soft components to form hybrid robotic systems,[48,49] wearable human exosuits driven by push–pull tendon actuators,[50,51] and hybrid designs for robot locomotion under challenging and transition zones between water, land, and air.[17,20] This suggests that the term ''soft'' robots should not be restrictive. Rather, the incorporation of many ''hard'' design features can unlock new potentials, leading to a new generation of hybrid soft robots that offer greater versatility and multifunctionality.

In this work, we seek to combine principled designs from both traditional hard and soft robot paradigms to achieve a new class of soft robots with simplified but reconfigurable robot kinematics. As shown in Figure 1a, our specific design approach is motivated by a broader class of robot mechanisms, called ''Soft Curved Reconfigurable Anisotropic Mechanisms'',[52–55] where discretized joint elements can be freely formed and separately controlled within a continuum

Downloaded by UNIVERSITY OF CALIFORNIA SAN DIEGO from www.liebertpub.com at 01/14/25. For personal use only.

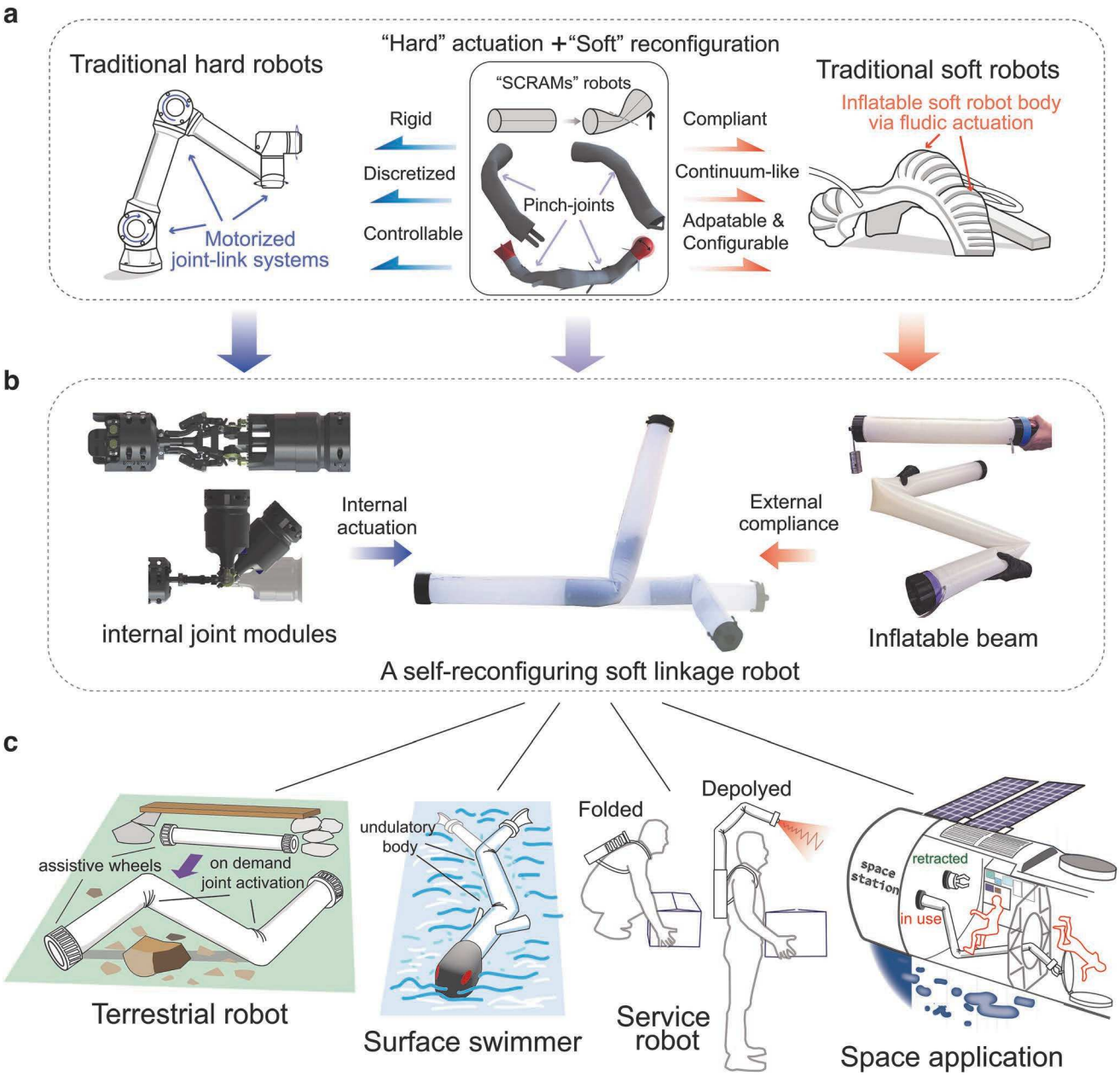

FIG. 1. A hybrid design approach of a reconfigurable soft linkage robot. **(a)** Design principles from traditional hard and soft robot archetypes, which are combined for a soft continuum robot with locally activated revolute joints (or ''pinch-joints'') for reconfigurable robot kinematics. **(b)** Specific rigid and soft robot components used in this work to build our proposed reconfigurable inflatable soft linkage robot. **(c)** Potential applications for the reconfigurable soft linkage robot. SCRAMs, Soft Curved Reconfigurable Anisotropic Mechanisms.

Downloaded by UNIVERSITY OF CALIFORNIA SAN DIEGO from www.liebertpub.com at 01/14/25. For personal use only.

soft robot body. The core of this approach is to achieve active shape control of locally induced curvatures, or ''pinches'' on planar materials, that exhibit anisotropic stiffness profiles and thus can be treated as effective revolute joints over different bending axes.[53,54]

This study presents a reconfigurable soft linkage robot, using a hybrid design method that combines both rigid and soft components, capable of on-demand joint creation and actuation (Fig. 1). Our robot is built from easily sealable and inflatable fabric beams with high strength-to-weight ratios, adjustable stiffnesses and shapes, as well as resistance to collisions.[32,56] For our proposed SCRAMs robot, instead of using permanently sealed joints,[57,58] we utilize temporary, adjustable ''pinch-joints'' that can be established and reset on-demand. These pinch-joints are made possible due to the easily pinchable and reconfigurable robot linkage housing internal motorized joint modules enabling on-demand robot joint–linkage kinematics as required (Fig. 1b). With a low body weight, a highly scalable form factor, and versatile configurations, our proposed robot is suitable for applications that involve transitioning between terrestrial and aquatic locomotion, assistance in daily human activities, and operation in challenging environments, such as low-gravity space (Fig. 1c).

In the following sections, we first discuss the design, fabrication, and reconfiguration process of our proposed reconfigurable soft linkage robot. We then characterize the pinch-joint mechanism by measuring the pinch force and variable stiffness based on different pinch geometries. The feasibility of our proposed internal motor-based joint actuation is analyzed considering the passive collapse strength of inflatable structures. With a single joint module and integrated pressure regulation, we highlight the three-dimensional (3D) reconfigurable robot workspace with relatively low error based on precalibrated open-loop signals. Finally, we demonstrate the robot as a terrestrial crawling robot with sequenced joint motions using different pinch-joint parameters (joint locations and axes).

Materials and Methods

System design of the reconfigurable soft linkage robot

Our proposed reconfigurable soft linkage robot was made of three main elements: a fabric-skinned inflatable body frame, preinserted joint modules featuring onboard control and power units, and a pressure regulation unit on one end of the robot (Fig. 2a; Supplementary Video S1). The robot body was created as an inflatable cylindrical beam using heat-sealable fabrics (200D and 420D TPU-coated nylon fabrics; Seattle Fabrics). Our robot's linkage body is customizable in various lengths and diameters to fit different deployable robot shapes. Both ends of the beam were sealed with rigid end caps: one end housed the pressure regulation unit, while the other had a removable cap to allow for the insertion of internal joint modules.

Each joint module was constructed within a cylinder of 35 cm (H) × 8 cm (D), enclosing all electromechanical components (including wires, boards, wireless modulus, motors, and batteries) inside a 3D-printed chassis (using polylactic acid). Due to the compact design space for the pinch-joint, we deliberately designed a tapered shape for the joint actuation part, and a slim structure (with only joint pinching mechanisms) for the joint formation part to fit inside the pinched robot joint region. These modules serve two functions: formation and actuation of pinch-joints (Fig. 2b). To form joints, a chain-climb mechanism was adopted for driving each module to the desired robot location, by meshing motorized 3D printed wheels (driven by Pololu geared DC motors, 1000:1, 6 V) with a ball chain. The ball chain was positioned along the central axis to avoid creating additional resistance when the joint is actuated.

We incorporated an assistive linear actuator (20D, 6 V with leadscrew transmission; Pololu) in the joint formation part to expand or retract the pinching mechanism to create fully deployed pinch joints with a 118 mm span (S) with a 40 mm width (W). Although variable pinch spans can be achieved via the continuous linear actuator, we tend to fully expand and retract the joint each time so that the pinch axis can be aligned with the joint axis for a minimized passive bending resistance. An assistive geared DC motor (1000:1, 6 V) was embedded to rotate the pinching mechanism to the desired joint axis. For pinch-joint actuation, two actuators (455:1 geared motors, 12 V; ServoCity) were mounted in the lengthwise direction of the beam on the opposite side of the joint module. A set of bevel gears (2:1 gear ratio; ServoCity) were connected to the motor shafts to convert torque into the right plane.

Figure 2c illustrates the robot's primary electronics and pressure controls, divided into three functional areas: joint formation, joint actuation, and pressure regulation. For joint formation, the assistive motors are powered by low-power drivers (MAX14870; Pololu), a Teensy-LC microcontroller, and a 7.4 V LiPo battery. In contrast, the more powerful joint actuators relied on high-power motor drivers (G2 18v17; Pololu), another Teensy-LC microcontroller, and an 11.1 V battery. Both microcontrollers drew power from its individual 3.7 V LiPo battery. Wireless modules (nRF24L01+) were used to enable remote motor control for both joint functions. These modules received commands based on feedback from encoders on each motor, processed via Proportional-Integral-Derivative (PID) controls. On one end of the robot, a pressure regulation unit was equipped with an air pump, a solenoid valve, and a pressure sensor (maximum 103 kPa; Honeywell), maintaining the robot's internal pressure using a PID algorithm. To prevent leakage during module insertion, a removable cap with an O-ring ensured a temporary seal.

Deployment and reconfiguration process of the robot

Our proposed robot can be deployed from a compact size with the robot's fabric body prestored in a chassis. A full robot deployment and reconfiguration process is showcased in Figure 3, where a single joint module was used to form pinch-joints at various locations and axes (Supplementary Video S2). In this setup, the module was prestored in a clear module chassis alongside the prefolded robot body. The robot was first inflated to 30 kPa using its onboard pressure regulation unit to allow the joint to self-enter into the soft linkage. As will be mentioned in the following section, creating a pinch-joint at a higher pressure state (e.g., greater 20 kPa) requires a significant amount of expansional force from the onboard motors. In this case, we briefly deflated to 5 kPa to enable the expansion of the pinching mechanism and then reinflated the robot to 30 kPa for joint actuation.

Our pinch-joints were capable of a full rotational movement approximately between −90° and +90° when pressurized

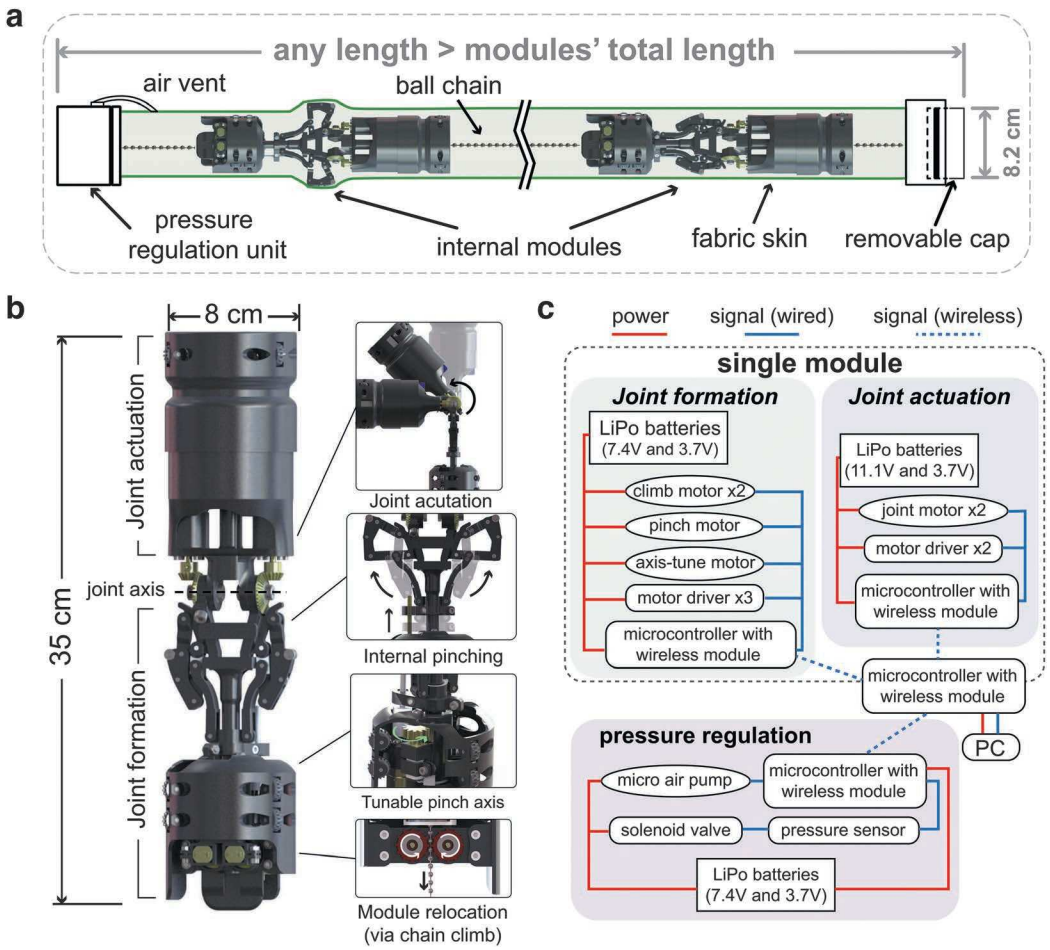

FIG. 2. Conceptual design of the entire reconfigurable robot, the internal joint module, and the electronics diagram. A mechanical design of the internal joint module. **(a)** A reconfigurable soft linkage robot system composition. **(b)** Internal joint module design with two parts: (1) joint formation, for relocating the module to the position (via chain/cable climbing), turning to the *right* pinch axis and expanding the linkage mechanism for pinch joint formation, and (2) joint actuation, for internally actuating the pinch-joints. **(c)** A diagram showing the main electronics (and fluidic control) used for both a single joint module and the pressure regulation of the entire robot.

(20–50 kPa). Precalibrated joint input signals, derived from both the motors' encoder readings and the actual pinch-joints' angular positions, were sent to the motors to guide the joint movements. Measurements (Supplementary Data) show that, after joint calibration, the joint was capable of reaching a desired location (mean error within 0.5°) repeatedly (1 standard deviation [SD] within 1°) under a 30 kPa internal pressure within a ±90° joint range. During operations, the actuated pinch-joint achieved rotations of about 0.9 rad/s at 30 kPa without bearing external loads. This sequence could be iteratively performed to achieve a myriad of joint configurations, thus enabling a versatile workspace.

Our current robot design faces challenges in lifting heavy loads due to potential collapsing of inflated cylindrical beams (explained in detail in later sections). When external loads exceed a certain threshold (e.g., due to internal joints moving or extra payloads), this may cause one joint module to buckle due to the offset moment generated by its adjacent joint modules or weights. In such instances, we can remodel the robot with an additional joint at the buckling point. The angular deflection at this new joint can be calculated based on the external moment and the beam's metrics (internal pressure and diameter), providing a more accurate approximation of the robot's kinematics under varying load conditions. However, for most use cases, we can deliberately space out our joints within a range of distances or simply apply the robot in a well-supported environment (e.g., ground or water) where the induced buckling torques (due to offset gravity) are externally countered.

Results

Passive mechanics of the pinch-joint mechanism

Understanding the passive mechanics of pinch-joints in an inflatable structure is critical for making informed design choices for this robot. For testing, we created a thin-membrane fabric beam (200-denier, heat sealable nylon, 0.3–0.4 mm in thickness; Seattle Fabrics) with a rounded cross-sectional area when inflated. As shown in Figure 4a, placing a rigid rod laterally inside the inflatable beam results in a pinched and ovalized cross section (due to the inextensible fabric wall). The rod must be longer in length than the circular cross-sectional diameter. We show that the

Downloaded by UNIVERSITY OF CALIFORNIA SAN DIEGO from www.liebertpub.com at 01/14/25. For personal use only.

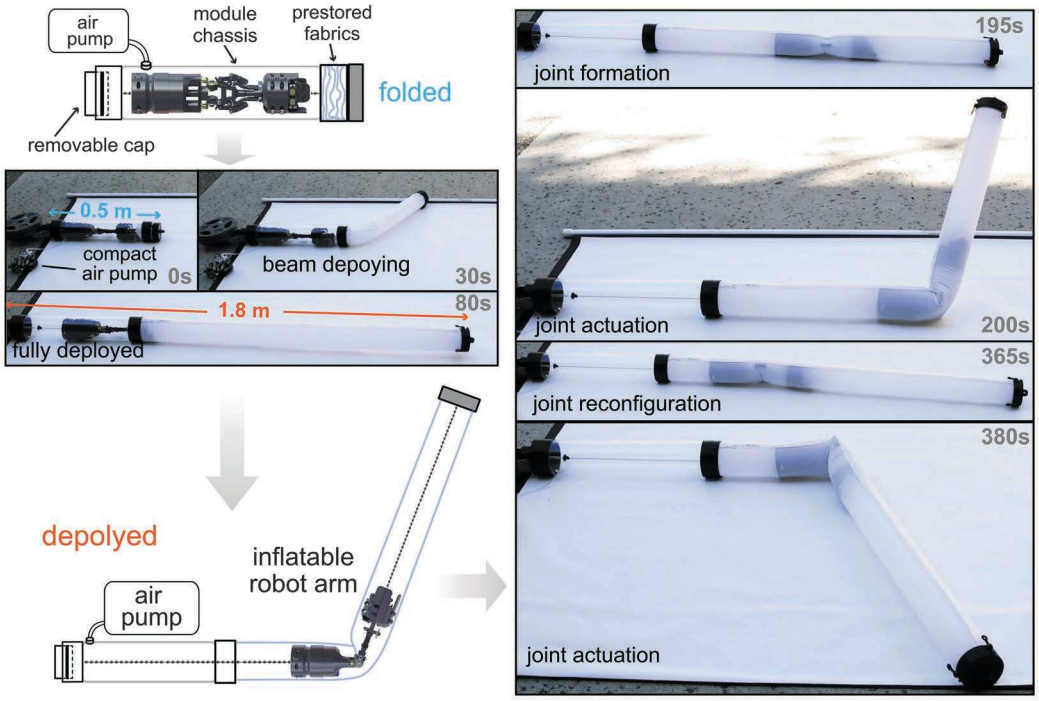

FIG. 3. Deployment and reconfiguring process of a compact soft linkage manipulator. The length of the retracted robot/module chassis was 0.5 m, with a fully deployed length of 1.8 m.

bending stiffness due to the separation of the continuous robot beam (Supplementary Data) can be significantly reduced based on certain pinch rod geometry.

To start, we measured the force required for creating and maintaining such a pinch using a materials testing apparatus (Fig. 4b; Supplementary Data). We noted that considerable extensional forces were required to create a pinch by moving two opposing sides of the circular cross section, even at low internal pressure levels (e.g., 100 N to form a 124 mm pinch span at 10 kPa). In general, the force necessary to establish a pinch in an inflated beam escalates with the increase of pinch spans and internal pressures. Considering the relatively high force requirement to create a pinch, we decide to modulate internal pressure for joint formation (robot deflation) and actuation (reinflation) as previously mentioned.

Next, we characterized the bending behaviors of the pinch-joints under different internal pressures. As illustrated in Figure 4c, we crafted different pinch spans by utilizing an internal pinch rod, and corresponding bending torques were recorded at varied levels of pressurization (Supplementary Data). Our results show that initial joint motion required a substantial torque, which can be attributed to a buckling instability common in inflated beams (Fig. 4d). As the bending angle increased (e.g., from 40° to 100°), the torque plateaued, and the two separated sections of the beam interfered deeper with each other, causing another increase in reactive torque at large joint angular deflections (e.g., over 100°). We also observed a diminished joint stiffness during the initial stages of joint motion when the pinch span was broadened to 106 mm.

In addition, extending the pinch span to 118 mm resulted in a significant torque decrease during the formation of the pinch-joint and across a large angular range. This drop in initial high stiffness is primarily due to the more ovalized pinch geometry of the cross section, which facilitates the beam to form wrinkles and bend more readily, lowering the reaction torques. As previously mentioned, our deployed robot pinch-joint replicates the geometry of the pinch rod that yields the lowest bending resistance [118 mm (S) × 40 mm (W)]. Each data point in this section represents the mean from five independent measurements, with the error bars standing for 1 SD. These experiments demonstrate the feasibility of developing mechanical revolute pinch-joints through the use of our proposed internal pinching mechanism.

Inflatable beam collapse strength versus internal joint torque

One of the considerations in using inflatable structures is the risk of ''collapse,'' a type of structural failure where a slight increase in load can lead to a significant increase in deflection. This is evident from the plateaued curve in previous joint stiffness tests and is caused by the inability of the composing membrane shell to resist compressive loads. As the external stress becomes zero on the concave side of the tube, the linkage starts to wrinkle, and with increasing external stress, the linkage is considered collapsed when the resultant zero stress propagates to either half[59,60] or all[61,62] of the structure's cross-sectional circumference. In this work, we choose the former case and the collapse moment can be described as follows:

$$M_c = \frac{\pi^2 p r^3}{4} \tag{1}$$

with M_c the critical collapse moment, p the beam's internal pressure, and r the radius of the inflated cylindrical cross-sectional area. Note that this model does not account for the

Downloaded by UNIVERSITY OF CALIFORNIA SAN DIEGO from www.liebertpub.com at 01/14/25. For personal use only.

Downloaded by UNIVERSITY OF CALIFORNIA SAN DIEGO from www.liebertpub.com at 01/14/25. For personal use only.

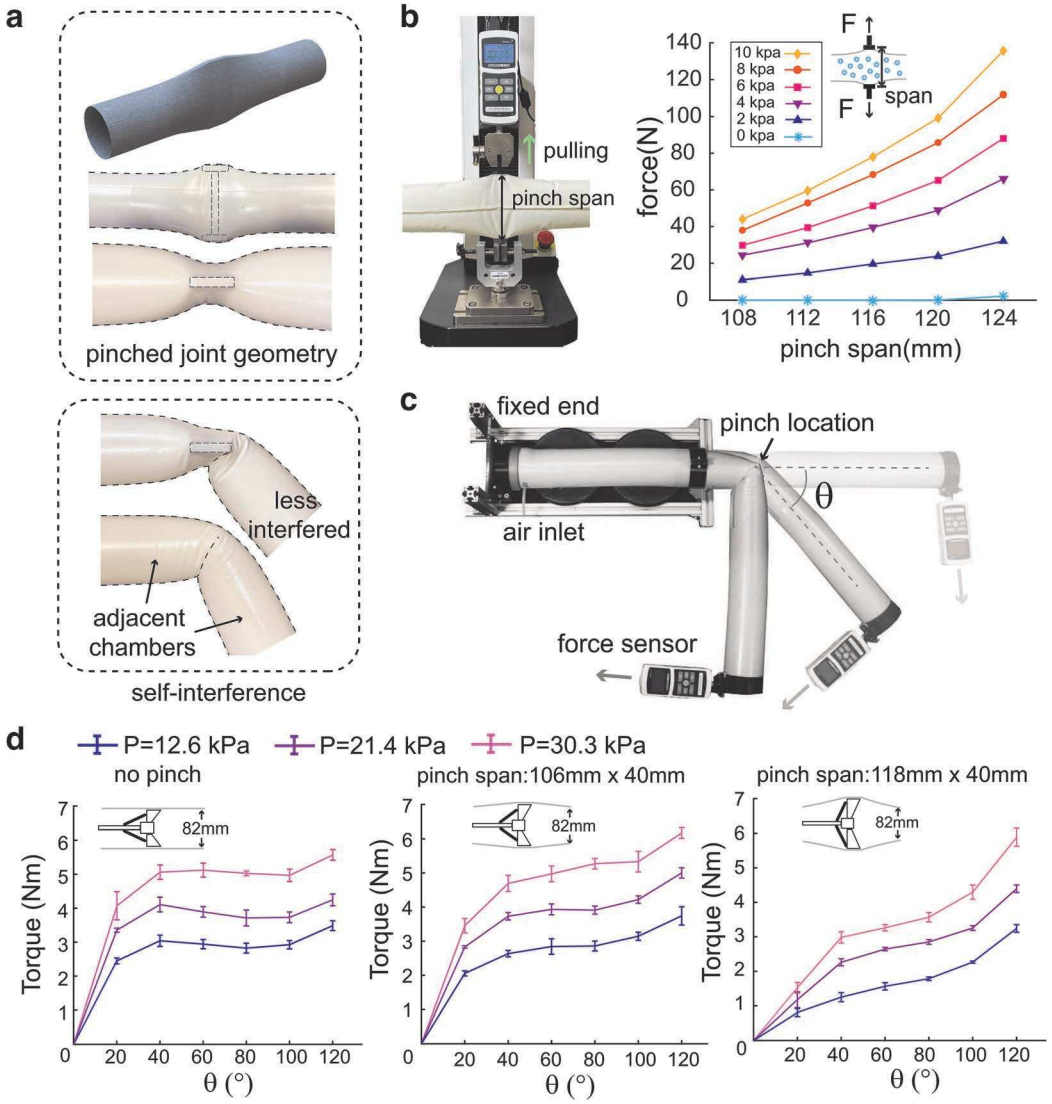

FIG. 4. Passive mechanics of the proposed pinch joint mechanism. **(a)** Real-world pictures showing the pinch-joint geometry. *Top images* show a pinch-joint from the *side* and *top view*. *Bottom images* compare a pinch-joint with (*upper image*) and without (*lower image*) an internal pinch rod. **(b)** Force requirement to form pinches under different pinch spans. **(c)** Experimental setup for testing the pinch-joint passive bending stiffness. **(d)** Torque–displacement relationships of a pinch-joint with different pinch geometries at different pressures.

thickness (t) change from overpressurization of the elastic thin wall structure and thus the stored strain energy.

The collapse model was validated through measurements of the bend angle of an inflated beam under increasing bending moments at the collapse point (Fig. 5a; Supplementary Data). As shown in Figure 5b, the measured collapse moments were found to align with the model in Eq. (1), although with a slight underestimation of the collapse moment for the highest pressure case (30.3 kPa), possibly due to the ignorance of the elastic energy stored in the fabric wall (error bars representing 1 SD over five independent trials).

Next, we briefly studied the torque requirement for driving these inflatables using internal motorized joint modules. As mentioned above, we installed our joint modules along the lengthwise direction of the inflatable beam, thus utilizing the compact design space for long high gear ratio DC motors (Fig. 5d). The relationship between the required torque from the internal joint modules and the beam collapse strength can be roughly confined between one and two folds of the beam's collapse moment (Fig. 5c), that is

$$M_c \leq T_j \leq 2M_c \tag{2}$$

Here, T_j represents the joint torque output from the internal joint modules. For the lower cap, the motor torque must surpass the inflatable beam's collapse moment to effectively drive the formed pinch-joint. In contrast, for the upper cap, additional joint torques are useful only up to the additional beam's collapse moment; beyond this, the beam risks collapsing at its other most vulnerable points (Fig. 3b).

Figure 5e displays a heat map of inflatables' collapse moments under different beam diameters and internal pressures. We selected a series of high torque density (Maxon GPX series; Supplementary Data) motors and plotted their

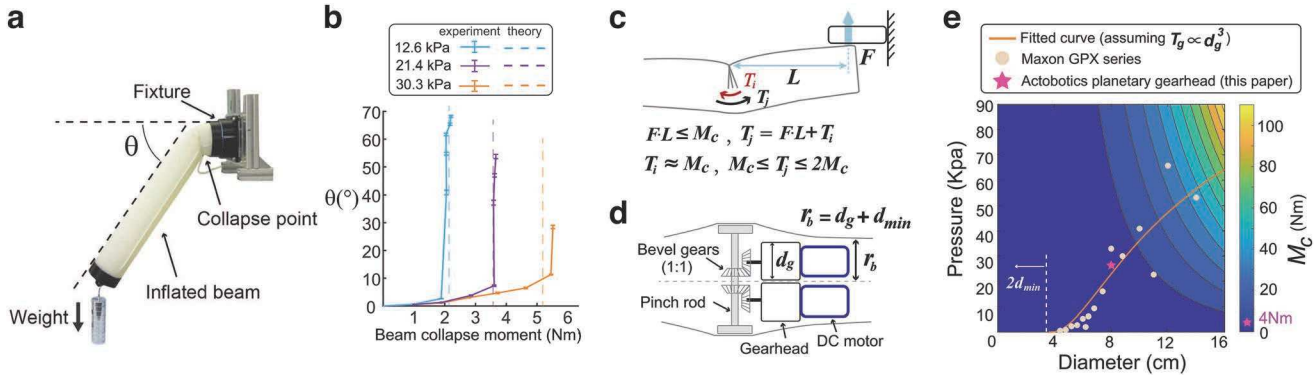

FIG. 5. Inflated robot linkage collapse strength and the practicability for internal joint actuation. **(a)** A schematic of the test rig for measuring the collapse states of an inflated beam. **(b)** Measured beam angular deflection with increasing loads with predicted collapse moments under different internal pressures. **(c)** A sketch showing an inflated robot linkage generating forces to the environment via internal joint torque inputs. **(d)** A schematic of the proposed solution for internal pinch joint actuation based on geared transmissions and motors installed in the longitudinal axis. **(e)** A design guidance for the internal joint actuation considering the upper bound scenario of the active joint output ($T_j = 2M_c$). The color map shows the collapse moments for inflated robot linkages with variable beam diameters and operational pressures. The *line* and *dots* are for design guidance indicating that the effective joint torque output after overcoming the beam collapse moment equals to one beam collapse moment ($T_j = 2M_c$).

specs on the heat map to indicate the internal operational beam pressure, the minimum beam diameter, and the associated joint torque output when capped by $T_j = 2M_c$ (Fig. 5c). A fitting curve is plotted assuming $T_g = kd_g^3$ (Tg – maximum continuous torque, and dg – gearhead diameter) while considering the geometric gap distance between the joint module's diameter and the robot's beam diameter (Supplementary Data). For our robot, we chose a set of geared DC motors (12 V, 26 RPM, 455:1; ServoCity) capable of a 4 Nm stall torque. We employed a set of 2:1 gear ratio bevel gears (32-pitch; ServoCity) to further increase the torque output. Our testing showed that our robot's collapse moment is $\sim$5 Nm at 30 kPa. It is important to note that the gap distance d_{min} (18 mm in this study) significantly impacts the allowable operating pressure and effective robot torque output, as unused design space could be utilized for electromagnetic (or other types of) actuation.

Demonstration of the reconfigurable robot kinematics

In this section, we aim to characterize our robot's reconfigurable workspace via a single pinch-joint setting under its different locations and joint axes. As displayed in Figure 6a, the robot was set up with its unactuated body vertically aligned, extending to a length of 1.3 m (with an internal pressure of 30 kPa). By sending commands to a single joint module within the robot's body to various positions (L_1 starting from the robot's base), we recorded the robot's kinematics by measuring the joint's positions and the robot's end tip in 3D. For each position of L_1, the joint's angles and axes were randomly altered. We tracked the robot using three infrared cameras (Prime 13 W; OptiTrack). The results, displayed in Figure 6b, show the robot's theoretical range of motion (dotted hemispheres) and real positions with black dots marking the joint locations and red dots indicating the robot's end tip. It was evident that for each L_1 position, the robot's movement forms a hemisphere. Moreover, as L_1 increases, this hemisphere narrows. Here, the joints are still commanded via precalibrated motor signals executed based on their own encoder readings.

Next, we measured the error of distance between the theoretical workspace and the real robot end tip position for different joint parameters. The average error of distance was about two orders of magnitude smaller than the robot's total length (Fig. 6c), which shows potentials for improved motion accuracy and repeatability of large-scale inflatable robots.

Finally, we measured the averaged energy consumption of the internal joint module for each different functionality (Fig. 6d). With the joint formed at relatively low internal pressures (e.g., 10 kPa), it required the least amount of energy to expand the internal pinching mechanism and to tune the joint axis. Similarly, the energy cost increased with increasing external load conditions exerted for functionalities, such as joint relocation and joint actuation. The values are reported in Figure 6d for different working conditions (each result was averaged over six individual measurements with the error bars for 1 SD).

A mobile reconfigurable terrestrial robot

Our robot demonstration showcases an untethered, dual-joint terrestrial robot with reconfigurable locomotion capabilities, allowing for a wide range of movements and adaptability. As shown in Figure 7a and b, a reconfigurable soft linkage robot [body length (L) $\times$ body width (BW), 1.3 m $\times$ 0.08 m] was inflated based on a 420 D, 0.4 mm fabric sheet with onboard pressure regulation units installed by one external end (Fig. 7a). The body was divided into three linkages via two embedded joint modules (J_1 and J_2) whose axes (φ_1 and φ_2) were perpendicular to each other. This was to create out-of-plane joint motions, which were translated into robot terrestrial locomotion (Fig. 7c, d). Here, we propose Gait 1 (''Shoulder-twist'') based on the shift of the center of mass (CoM) of either joint and Gait 2 (''Arm-paddling'') based on the shift of the CoM of the robot's outer linkages.

To further explore the robot gait performance, we conducted experiments by tracking the robot's two-dimensional (x–y) position and change of orientation ($\Delta\alpha$) by varying the linkage distributions of the robot and with different gaits

Downloaded by UNIVERSITY OF CALIFORNIA SAN DIEGO from www.liebertpub.com at 01/14/25. For personal use only.

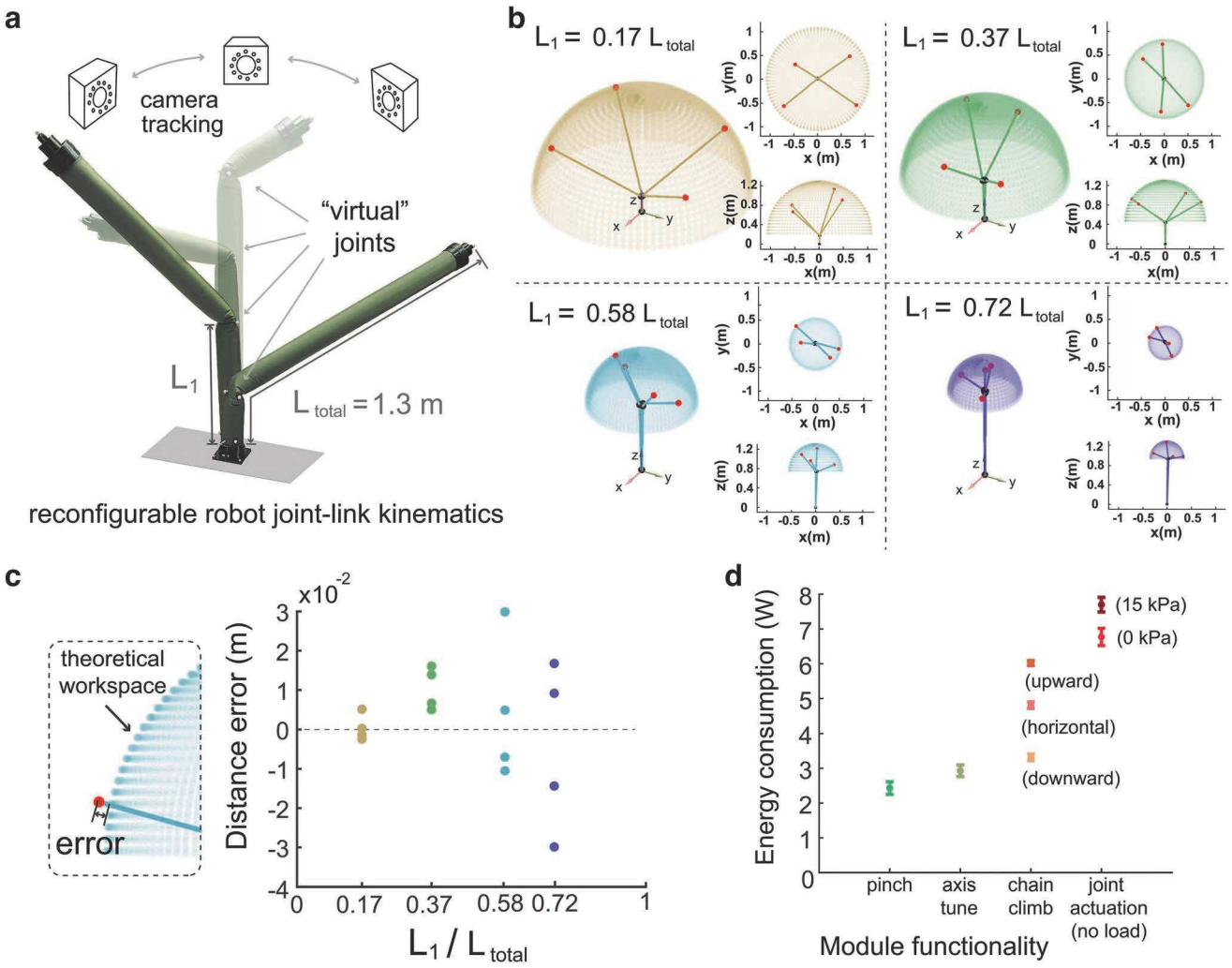

FIG. 6. Reconfigurable ''rigid'' kinematics of the proposed soft linkage robot. **(a)** Experimental setup for tracking the reconfigurable robot kinematics. Image overlay shows four different configurations of link length, joint axis orientation, and joint bend angle. **(b)** Reconfigurable workspace and measured geometric states for the robot with different joint locations (L_1). **(c)** Error of distance between the theoretical workspace and the measured end tip position. **(d)** Energy consumptions for each individual functionality of the internal joint module.

(Supplementary Videos S4 and S5). As shown in Figure 7c, and Supplementary Video S3, the two joints (perpendicularly aligned) were driven by signals with the same amplitude (±45°, out-of-phased, with a cycle of 13.4 s and a 4.2 s phase shift) at two different joint locations as Configuration 1 (0.36:0.33:0.31) and Configuration 2 (0.28:0.51:0.21). For Gait 1, a series of time-lapsed robot positions and orientations were plotted (each separated by a constant time interval) with the green bar representing the robot's central linkage and the dots as joint markers (circles for J1 and solid dots for J2, with the orange dots as indicating the middle of the two). It can be seen that changing the robot's side arm length distribution reduced the robot's linear traveling speed only by a slight amount (from 0.26 to 0.24 BL/step, 5 to 4.6 cm/s). The robot's orientation maintained relatively constant for Configuration 2 but tended to drift toward the short arm side for Configuration 1 (4°/step).

To compare the linear traveling speeds between the two gaits, we did an experiment where the robot switched its gait in the middle of a successive rolling motion (Supplementary Video S4). As shown in Figure 7d, with the same joint input signals for both gaits (unchanged from the previous test), Gait 1 was faster than Gait 2 (0.24 BL/step vs. 0.18 BL/step, 4.5 cm/s vs. 3.4 cm/s) and the body orientation seemed more steady in Gait 1. This may be due to the fact as Gait 2 (''arm-paddling'') can be simplified as pure rolling of the center linkage, Gait 1 involved lifting its central linkage off the ground, and for each step, it resulted in a linear body translation, which was amplified by the length of the side arms. Note that in this experiment, the robot's gait transition from Gait 2 to Gait 1 happened due to emerging environmental conditions where Gait 2 was incapable of rolling the robot forward.

These were all done without deliberately changing the joint input signals, indicating a sign of self-adaptive robot locomotion for the given robot joint–linkage configuration. Finally, we performed an experiment demonstrating the robot's turning capability based on differential joint inputs and linkage distributions (Supplementary Video S5). Here, we set

Downloaded by UNIVERSITY OF CALIFORNIA SAN DIEGO from www.liebertpub.com at 01/14/25. For personal use only.

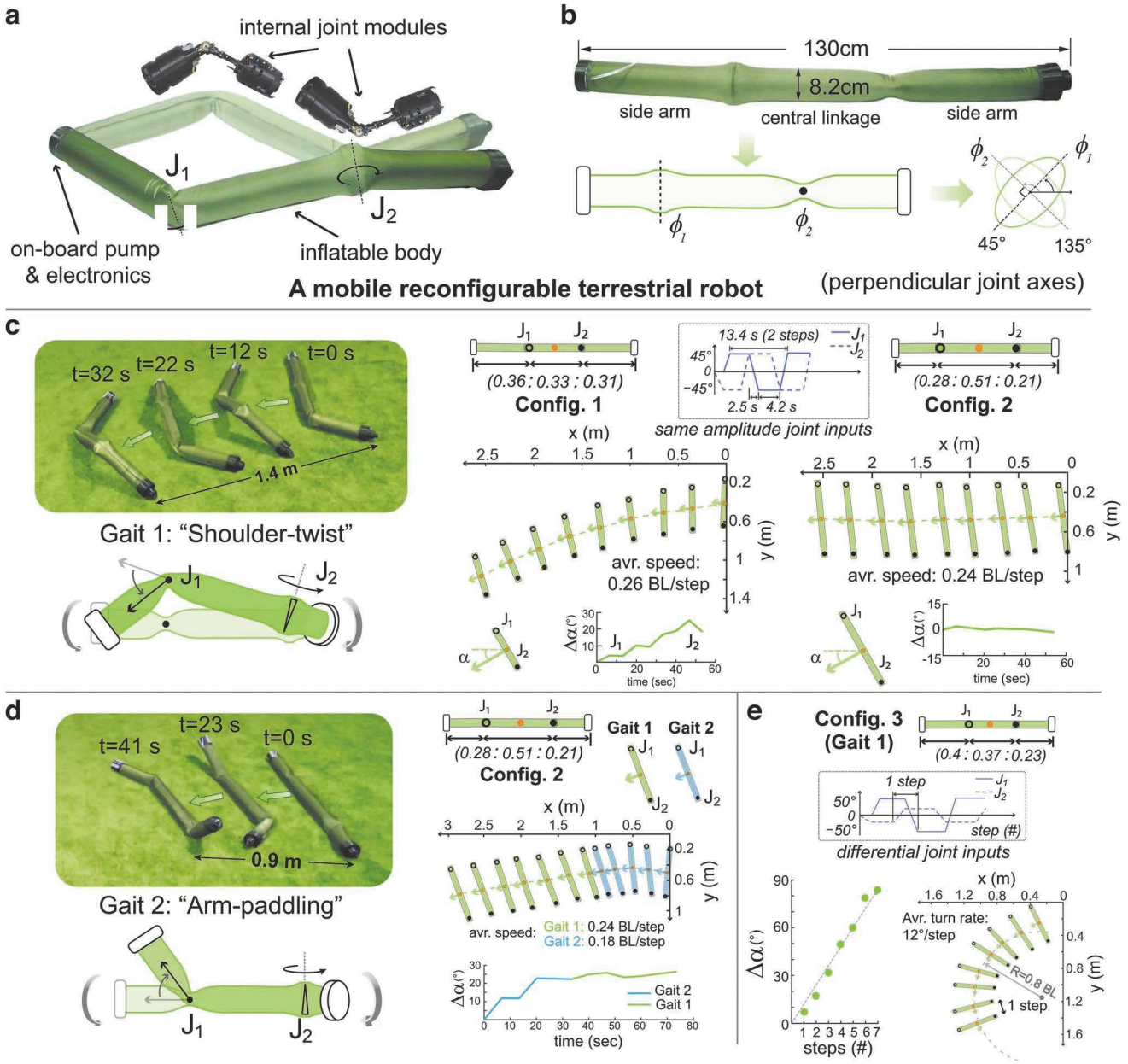

FIG. 7. A mobile reconfigurable terrestrial robot with two pinch joints. **(a)** A picture of the robot with onboard electronics, a pump, and embedded joint modules. **(b)** The joints were poised with their axes perpendicular to each other. **(c)** Robot locomotion and time-lapsed recording of the robot traveling on land (artificial turf) based on Gait 1, where the joints acted as shoulders twisting for robot rolling motion. **(d)** Robot locomotion based on Gait 2, using the shifted center of mass of the side arms to generate rolling torque. A transition from Gait 2 to Gait 1 was recorded, and the joints were actuated based on the same amplitudes and phase shift as in **c**. **(e)** Robot turning with differential link distributions and joint signals between J1 and J2 using Gait 1.

J1 with a ±50° motion amplitude and ±25° for J2 under Configuration 3, with an even shifted length distribution (0.4:0.37:0.23). As shown in Figure 7e, the robot turned at a rate of 12° per step, with each step representing half of the complete robot rolling cycle. The estimated turning radius was about 0.8 robot body length, which was a sharp improvement from changing only the distributed arm lengths (with similar joint signals for both joints).

In this study, we noticed that different joint locations (and their mass shifts) may affect the robot's dynamic behaviors during locomotion. For the shoulder-twist gait (Gait 1), maintaining evenly distributed linkages results in optimal travel speed. When the side arms are disproportionately short, the speed decreases. For the arm-paddling gait (Gait 2), the length distribution of the linkages is less critical as this gait relies on rolling motion, with the robot's mass center always on the ground. Finally, for both cases, having a longer arm length on either side makes the robot veer away from that side (e.g., a longer left side arm will make the robot turn right).

Downloaded by UNIVERSITY OF CALIFORNIA SAN DIEGO from www.liebertpub.com at 01/14/25. For personal use only.

To conclude, this section serves as an initial proof of concept of a potential terrestrial robot application for our proposed reconfigurable soft linkage robot. The proposed gait cycles can be utilized for traveling on normal terrains, and a robot reorientation strategy was explored based on different joint–linkage configurations. In the future, we will explore more joint–linkage configurations (joint axes and locations) and their potential gait strategies for adapting to multi-environment working conditions. Robot transition over different environments (e.g., land to water and vice versa) will also be our main focus for suitable reconfigurable robot locomotion strategies.

Conclusions

This study presents a hybrid design of an inflatable soft linkage robot with adaptable joint–linkage kinematics. Our robot features a deployable inflatable body actuated by internal motorized pinch-joint modules. We delve into its design, reconfiguration, pinch force requirements, variable joint stiffness, actuation feasibility within an inflatable structure, reconfigurable kinematics, and demonstrations of its locomotion with various joint configurations.

Our approach fits in the broader concept of soft curved reconfigurable anisotropic mechanisms (SCRAMs),[52,53,55] which use geometric pinching in compliant structures to produce anisotropic joint stiffness. This innovation is driven by the desire to advance beyond the constraints of fixed robot joint–linkage designs. Our technique allows adaptable robot workspaces, kinematics, and dynamics[63] without the typical redundancy seen in self-reconfigurable modular robotics.[64] The SCRAMs concept is versatile, unrestricted by choices of material, actuation, or sensing. For instance, SCRAM robot embodiments have been crafted using 3D-printed materials,[53] integrated optical and flex sensors,[65] diverse joint actuation methods,[55,66] and theoretical frameworks to predict ''virtual'' joint behaviors through simulations and geometric techniques.[67]

One design challenge for this robot is the overall coordination between a connected robot body chamber and the control of independently created pinch-joints. The connectivity of the inner robot body indicates a global pressure that may affect the formation and retraction of multiple joints (e.g., joint forming sequences). Meanwhile, for future robot multi-joint collaboration, we assume each motorized joint module has distance sensors (e.g., optical sensors) measuring its relative positions inside the robot's body. An absolute encoder measures each joint's axis angle as well as Inertial Measurement Units on the two ends of the robot measuring its orientation with regard to the global coordinate. A simplified kinematic model can be established via these sensor inputs and a centralized robot operating platform (e.g., Robot Operating System 2). For additional shape sensing of small beam curvatures, we tend to embed local flexible sensors with predefined patterns.[68] However, addressing the trade-off between sensing resolution and mechanical complexity remains essential in future research.[69]

In summary, this work presents a novel hybrid design approach for creating reconfigurable robots with inflatable body frames and simplified joint–linkage kinematics enabled by internal joint actuation. This approach offers numerous potential applications in challenging and unstructured environments such as low-gravity space and extraterrestrial terrains, where adaptability, weight, and deployability are crucial. The proposed hybrid design can serve as a foundation for future functional robots requiring easily deployable, adaptive, and controllable behaviors for diverse environments and multifunctional tasks.

Authors' Contributions

M.J. and N.G. conceived the conceptual designs of the robot and the experiments, M.J. designed the internal joint module, M.J. and J.W. fabricated the robot and conducted the experiments, M.J. and N.G. analyzed the results and wrote the study. All authors reviewed the study.

Author Disclosure Statement

No competing interests to disclose.

Funding Information

Funding support was provided through the Department of Mechanical and Aerospace Engineering at the University of California San Diego. This material was based on work supported by the National Science Foundation under Grant No. 1935324. Any opinions, findings, and conclusions, or recommendations expressed in this material are those of the author(s) and do not necessarily reflect the views of the National Science Foundation.

Supplementary Material

Supplementary Data
Supplementary Video S1
Supplementary Video S2
Supplementary Video S3
Supplementary Video S4
Supplementary Video S5

References

1. Almurib HAF, Al-Qrimli HF, Kumar N. A review of application industrial robotic design. In: 2011 Ninth International Conference on ICT and Knowledge Engineering, Bangkok, Thailand; 2012; pp. 105–112; doi: 10.1109/ICTKE.2012.6152387
2. Pervozvanski AA, Freidovich LB. Robust stabilization of robotic manipulators by PID controllers. Dyn Control 1999; 9(3):203–222.
3. Greco C, Kotak P, Pagnotta L, et al. The evolution of mechanical actuation: From conventional actuators to artificial muscles. Int Mater Rev 2022;67(6):575–619.
4. Guo W, Li R, Cao C, et al. Kinematics, dynamics, and control system of a new 5-degree-of-freedom hybrid robot manipulator. Adv Mech Eng 2016;8(11):1687814016680309.
5. Vukobratovic M, Tuneski A. Adaptive control of single rigid robotic manipulators interacting with dynamic environment—An overview. J Intell Rob Syst 1996;17(1): 1–30.
6. Murtaza MA, Aguilera S, Waqas M, et al. Safety compliant control for robotic manipulator with task and input constraints. IEEE Robot Autom Lett 2022;7(4):10659–10664.
7. Whitesides GM. Soft robotics. Angew Chem Int Ed Engl 2018;57(16):4258–4273.
8. Schmitt F, Piccin O, Barbé L, et al. Soft robots manufacturing: A review. Front Robot AI 2018;5:84.

Downloaded by UNIVERSITY OF CALIFORNIA SAN DIEGO from www.liebertpub.com at 01/14/25. For personal use only.

Downloaded by UNIVERSITY OF CALIFORNIA SAN DIEGO from www.liebertpub.com at 01/14/25. For personal use only.

9. Xavier MS, Tawk CD, Zolfagharian A, et al. Soft pneumatic actuators: A review of design, fabrication, modeling, sensing, control and applications. IEEE Access 2022;10: 59442–59485.
10. Booth JW, Cyr-Choinière O, Case JC, et al. Surface actuation and sensing of a tensegrity structure using robotic skins. Soft Robot 2021;8(5):531–541.
11. Kar D, George B, Sridharan K. A review on flexible sensors for soft robotics. In: Systems for Printed Flexible Sensors: Design and Implementation. (Islam T, Mukhopadhyay S, George B. eds.). IOP Publishing: Bristol; 2022.
12. Thuruthel TG, Shih B, Laschi C, et al. Soft robot perception using embedded soft sensors and recurrent neural networks. Sci Robot 2019;4(26):eaav1488; doi: 10.1126/scirobotics .aav1488
13. El-Atab N, Mishra RB, Al-Modaf F, et al. Soft actuators for soft robotic applications: A review. Adv Intell Syst 2020; 2(10):2000128.
14. Li M, Pal A, Aghakhani A, et al. Soft actuators for real-world applications. Nat Rev Mater 2022;7:235–249.
15. Shepherd RF, Ilievski F, Choi W, et al. Multigait soft robot. Proc Natl Acad Sci U S A 2011;108(51):20400–20403.
16. Polygerinos P, Wang Z, Overvelde JTB, et al. Modeling of soft fiber-reinforced bending actuators. IEEE Trans Rob 2015;31(3):778–789.
17. Hwang D, Barron EJ 3rd, Haque ABMT, et al. Shape morphing mechanical metamaterials through reversible plasticity. Sci Robot 2022;7(63):eabg2171.
18. Buckner TL, Bilodeau RA, Kim SY, et al. Roboticizing fabric by integrating functional fibers. Proc Natl Acad Sci U S A 2020;117(41):25360–25369.
19. Manti M, Cacucciolo V, Cianchetti M. Stiffening in soft robotics: A review of the state of the art. IEEE Robot Autom Mag 2016;23(3):93–106.
20. Baines R, Patiballa SK, Booth J, et al. Multi-environment robotic transitions through adaptive morphogenesis. Nature 2022;610(7931):283–289.
21. Ju Y, Hu R, Xie Y, et al. Reconfigurable magnetic soft robots with multimodal locomotion. Nano Energy 2021;87: 106169.
22. Katzschmann RK, DelPreto J, MacCurdy R, et al. Exploration of underwater life with an acoustically controlled soft robotic fish. Sci Robot 2018;3(16):aar3449; doi: 10 .1126/scirobotics.aar3449
23. Hegde C, Su J, Tan JMR, et al. Sensing in soft robotics. ACS Nano 2023;17(16):15277–15307; doi: 10.1021/ acsnano.3c04089
24. Araromi OA, Graule MA, Dorsey KL, et al. Ultra-sensitive and resilient compliant strain gauges for soft machines. Nature 2020;587(7833):219–224.
25. Must I, Sinibaldi E, Mazzolai B. A variable-stiffness tendril-like soft robot based on reversible osmotic actuation. Nat Commun 2019;10(1):1–8.
26. Rus D, Tolley MT. Design, fabrication and control of origami robots. Nat Rev Mater 2018;3(6):101–112.
27. Ebrahimi N, Bi C, Cappelleri DJ, et al. Magnetic actuation methods in bio/soft robotics. Adv Funct Mater 2021; 31(11):2005137.
28. Kim Y, Parada GA, Liu S, et al. Ferromagnetic soft continuum robots. Sci Robot 2019;4(33):eaax7329; doi: 10 .1126/scirobotics.aax7329
29. Sanan S, Moidel JB, Atkeson CG. Robots with Inflatable Links. In: 2009 IEEE/RSJ International Conference on Intelligent Robots and Systems. 2009; pp. 4331–4336.
30. Xiong J, Chen J, Lee PS. Functional fibers and fabrics for soft robotics, wearables, and human-robot interface. Adv Mater 2021;33(19):e2002640.
31. Wang W, Kim N-G, Rodrigue H, et al. Modular assembly of soft deployable structures and robots. Mater Horiz 2017; 4(3):367–376.
32. Palmieri P, Melchiorre M, Mauro S. Design of a lightweight and deployable soft robotic arm. Robotics 2022; 11(5):88.
33. Shah DS, Powers JP, Tilton LG, et al. A soft robot that adapts to environments through shape change. Nat Mach Intell 2020;3(1):51–59.
34. Hawkes EW, Blumenschein LH, Greer JD, et al. A soft robot that navigates its environment through growth. Sci Robot 2017;2(8):aan3028; doi: 10.1126/scirobotics.aan3028
35. da Veiga T, Chandler JH, Lloyd P, et al. Challenges of continuum robots in clinical context: a review. Prog Biomed Eng 2020;2(3):032003.
36. Park M, Jeong B, Park Y-L. Hybrid system analysis and control of a soft robotic gripper with embedded proprioceptive sensing for enhanced gripping performance. Adv Intell Syst 2021;3(3):2000061.
37. Yap HK, Ng HY, Yeow C-H. High-force soft printable pneumatics for soft robotic applications. Soft Robot 2016; 3(3):144–158.
38. Drotman D, Jadhav S, Sharp D, et al. Electronics-free pneumatic circuits for controlling soft-legged robots. Sci Robot 2021;6(51):eaay2627; doi: 10.1126/scirobotics.aay2627
39. Hartmann F, Baumgartner M, Kaltenbrunner M. Becoming sustainable, the new frontier in soft robotics. Adv Mater 2021;33(19):e2004413.
40. Lipson H. Challenges and opportunities for design, simulation, and fabrication of soft robots. Soft Robot 2014;1(1): 21–27.
41. Zhang Y, Li P, Quan J, et al. Progress, challenges, and prospects of soft robotics for space applications. Adv Intell Syst 2023;5(3):2200071; doi: 10.1002/aisy.202200071
42. Galloway KC, Polygerinos P, Walsh CJ, et al. Mechanically programmable bend radius for fiber-reinforced soft actuators. In: 2013 16th International Conference on Advanced Robotics (ICAR). 2013; pp. 1–6.
43. Pagoli A, Chapelle F, Corrales-Ramon J-A, et al. Review of soft fluidic actuators: Classification and materials modeling analysis. Smart Mater Struct 2021;31(1):013001.
44. Kokubu S, Wang Y, Tortós Vinocour PE, et al. Evaluation of fiber-reinforced modular soft actuators for individualized soft rehabilitation gloves. Actuators 2022;11(3):84.
45. Wang X, Mao G, Ge J, et al. Untethered and ultrafast soft-bodied robots. Commun Mater 2020;1(1):1–10.
46. Gu G-Y, Zhu J, Zhu L-M, et al. A survey on dielectric elastomer actuators for soft robots. Bioinspir Biomim 2017; 12(1):011003.
47. Usevitch NS, Hammond ZM, Schwager M, et al. An untethered isoperimetric soft robot. Sci Robot 2020;5(40): aaz0492; doi: 10.1126/scirobotics.aaz0492
48. Stokes AA, Shepherd RF, Morin SA, et al. A hybrid combining hard and soft robots. Soft Robot 2014;1(1):70–74.
49. Haggerty DA, Naclerio ND, Hawkes EW. Hybrid vine robot with internal steering-reeling mechanism enhances system-level capabilities. IEEE Robot Autom Lett 2021; 6(3):5437–5444.
50. Nuckols RW, Lee S, Swaminathan K, et al. Individualization of exosuit assistance based on measured muscle dynamics during versatile walking. Sci Robot 2021;6(60):eabj1362.

51. Asbeck AT, De Rossi SMM, Galiana I, et al. Stronger, smarter, softer: Next-generation wearable robots. IEEE Robot Autom Mag 2014;21(4):22–33.
52. Sharifzadeh M, Jiang Y, Aukes DM. Reconfigurable curved beams for selectable swimming gaits in an underwater robot. IEEE Robot Autom Lett 2021;6(2):3437–3444.
53. Jiang M, Yu Q, Gravish N. Vacuum induced tube pinching enables reconfigurable flexure joints with controllable bend axis and stiffness. In: 2021 IEEE 4th International Conference on Soft Robotics (RoboSoft). 2021; pp. 315–320.
54. Jiang Y, Sharifzadeh M, Aukes DM. Reconfigurable soft flexure hinges via pinched tubes. In: 2020 IEEE/RSJ International Conference on Intelligent Robots and Systems (IROS). 2020; pp. 8843–8850.
55. Sparks C, Justus N, Hatton R, et al. Amoeba-inspired swimming through isoperimetric modulation of body shape. In: 2022 IEEE/RSJ International Conference on Intelligent Robots and Systems (IROS). 2022; pp. 2685–2692.
56. Voisembert S, Mechbal N, Riwan A, et al. Design of a novel long-range inflatable robotic arm: Manufacturing and numerical evaluation of the joints and actuation. J Mech Robot 2013;5(4):045001.
57. Voisembert S, Riwan A, Mechbal N, et al. A novel inflatable robot with constant and continuous volume. In: 2011 IEEE International Conference on Robotics and Automation. 2011; pp. 5843–5848.
58. Satake Y, Ishii H. Pitch-up motion mechanism with heat welding by soft inflatable growing robot. IEEE Robot Autom Lett 2022;7(2):5071–5078.
59. Thomas J-C, Wielgosz C, Le Van A. Mechanics of inflatable fabric beams. In: 4th International Conference on Thin Walled Structures (ICTWS'04), Loughborough, United Kingdom; June 2004; p. hal-01008403.
60. Thomas J-C, Bloch A. Non linear behaviour of an inflatable beam and limit states. Procedia Eng 2016;155:398–406.
61. Karam GN, Gibson LJ. Elastic buckling of cylindrical shells with elastic cores—I. Analysis. Int J Solids Struct 1995;32(8):1259–1283.
62. Main JA, Peterson SW, Strauss AM. Load-deflection behavior of space-based inflatable fabric beams. J Aerosp Eng 1994;7(2):225–238.
63. Seo J, Paik J, Yim M. Modular reconfigurable robotics. Annu Rev Control Robot Auton Syst 2019;2(1):63–88.
64. Chennareddy SSR, Agrawal A, Karuppiah A. Modular self-reconfigurable robotic systems: A survey on hardware architectures. J Robot 2017;2017; doi: 10.1155/2017/5013532
65. Harnett CK. Soft Optics with Mechanically Tunable Refractive Index. US Patent; 2021.
66. Bupe P, Jackson DJ, Harnett CK. Electronically reconfigurable virtual joints by shape memory alloy-induced buckling of curved sheets. In: SoutheastCon 2022. 2022; pp. 598–604.
67. Hatton RL, Choset H. Geometric swimming at low and high reynolds numbers. IEEE Trans Rob 2013;29(3):615–624.
68. Wang Y, Nitta T, Hiratsuka Y, et al. In situ integrated microrobots driven by artificial muscles built from biomolecular motors. Sci Robot 2022;7(69):eaba8212.
69. Su H, Hou X, Zhang X, et al. Pneumatic soft robots: Challenges and benefits. Actuators 2022;11(3):92.

Address correspondence to:
Nicholas Gravish
Department of Mechanical and Aerospace Engineering
University of California San Diego
La Jolla, CA 92093
USA

E-mail: ngravish@eng.ucsd.edu

Downloaded by UNIVERSITY OF CALIFORNIA SAN DIEGO from www.liebertpub.com at 01/14/25. For personal use only.